Applied Thermal Engineering 65 (2014) 94–101

Contents lists available at ScienceDirect

Applied Thermal Engineering

journal homepage: www.elsevier.com/locate/apthermeng

Net thermoelectric generator power output using inner channel geometries with alternating flow impeding panels

Calil Amaral [a], Caio Brandão [b], Éric V. Sempels [c], Frédéric J. Lesage [d,e,*]

[a] Universidade Federal de Uberlândia, 2121 Av. João Naves de Ávila, Uberlândia 38-408-290, Brazil
[b] Carleton University, 1125 Colonel By Drive, Ottawa K1S 5B6, Canada
[c] École Polytechnique de Montréal, 2900 Boulevard Edouard-Montpetit, Montréal H3T 1J4, Canada
[d] Cégep de l'Outaouais, 333 boul. de la Cité-des-Jeunes, Gatineau J8Y 6M4, Canada
[e] McMaster University, 1280 Main Street West, Hamilton L8S 4L7, Canada

HIGHLIGHTS

- Inner flow impedance enhancing thermal transport increases thermoelectric power.
- Test cases include constant thermal input conditions for varying flow rates.
- Optimal insert geometry with alternating flow impeding panels is investigated.
- Net thermoelectric power accounting for pumping penalty is measured and discussed.

ARTICLE INFO

Article history:
Received 30 September 2013
Accepted 17 December 2013
Available online 9 January 2014

Keywords:
Thermoelectric generator
Waste heat recovery
Flow impeding geometries
Pressure drop
Thermal transport enhancement

ABSTRACT

Due to an abundance of low cost waste-heat in the industrial and residential sector, many studies in recent years have focused on applications of low grade heat for local energy needs. These include heat reutilization, thermal conversion to mechanical energy and thermal conversion to electricity. The thermoelectric effect presents a promising potential for effective conversion of low grade waste-heat yet is currently limited in application due to a conversion efficiency that is not cost effective. The present work focuses on mechanical methods to improve the thermal tension driving the electromotive force responsible for thermoelectric power production. More specifically, flow impeding geometries are inserted into the flow channels of a liquid-to-liquid thermoelectric generator thereby enhancing the heat transfer near its embedded thermoelectric modules. Consequentially, the thermal dipole across the modules is increased improving the overall power output. Care is taken to measure the adverse pressure drop caused by the use of the flow impeding geometries in order to evaluate the net power output. This net thermoelectric power output is measured, reported and discussed for a fixed inlet temperature difference, a fixed electrical load, varying flow rates and varying insert geometries.

1. Introduction

The conversion of thermal energy to electricity has been the subject of many recent investigations due to an excess of unused residential and industrial waste-heat. The state of the art of currently available conversion technologies is limited in its efficiency making the exploitation of low cost residual heat non-economically viable. Indeed, Wu [1] presents thermoelectric heat recovery as a promising avenue for power generation while highlighting that it requires further advancements in system conversion efficiency in order to render the process cost effective. To this end, efforts to improve the conversion efficiency of practical applications of this phenomenon, known as the Seebeck effect, focus on material and module design and on thermal system management.

Thermoelectric material and module design investigations seek to improve the thermopower production of thermoelectric elements. In these studies, thermopower is measured in terms of the Seebeck coefficient which quantifies the ratio of the electric potential across an element with the difference in temperature at the element's extremities. It represents the ratio of the charge carrier's transported entropy to its charge in an asymmetric thermal field. Since it is the asymmetric nature of this thermal dipole that is

* Corresponding author. Cégep de l'Outaouais, 333 boul. de la Cité-des-Jeunes, Gatineau J8Y 6M4, Canada. Tel.: +1 819 770 4012; fax: +1 819 770 8167.
E-mail addresses: frederic.j.lesage@gmail.com, Frederic.Lesage@cegepoutaouais.qc.ca (F.J. Lesage).

1359-4311/$ – see front matter © 2013 Elsevier Ltd. All rights reserved.
http://dx.doi.org/10.1016/j.applthermaleng.2013.12.044

Nomenclature

Symbol

c_p	Specific heat at constant pressure, J/kg K
D_p	Linear panel density, panels/m
k	Thermal conductivity, W/m K
n	Number of channels
p	Pressure, PSI
P	Power, W
$\bar{P}$	Net power, W
T	Temperature, K
TEG	Thermoelectric generator
TEM	Thermoelectric module
$\dot{V}$	Volumetric flow rate, m^3/s
$\dot{W}$	Work due to pressure drop, W

Greek letters

α	Seebeck coefficient, V/K
η	Conversion efficiency
ρ	Fluid density, kg/m^3
σ	Electrical conductivity, S/m

Subscripts

C	cold side
ch	channel
H	hot side
in	inlet
out	outlet

responsible for generating the electromotive force which mobilizes the carriers, the element's ability to conduct electricity relative to its ability to conduct heat dictates its thermal to electricity conversion efficiency. This is measured in terms of the dimensionless Figure-of-Merit *ZT* (e.g., [2]) which is dependent on temperature *T*, material electrical conductivity σ, material thermal conductivity k and the Seebeck coefficient α, such that

$$ZT = \frac{\alpha\sigma T}{k}. \quad (1)$$

The goal of thermoelectric design studies is to maximize a material's dimensionless Figure-of-Merit in which *ZT* values greater than unity is indicative of a material with a promising ability to convert thermal energy to electricity.

Conventional wisdom is that thermoelectric modules have the greatest potential for application with low cost heat sources in a temperature range below 450 K. In this range, commercially available thermoelectric modules have embedded semiconductors based on the alloy bismuth (Bi) combined with the alloys antimony (Sb), selenium (Se), and tellurium (Te) (e.g., [2]). Recent advancements have improved the *ZT* values of thermoelectric materials for target temperature ranges by investigating novel alloy combinations and semiconductor compositions (e.g., [3,4]). Similarly, some studies aim to improve thermoelectric efficiency through innovative module design in which geometric enhancement methods are investigated and segmented thermoelectric elements are combined in an effort to increase charge carrier concentration (e.g., [5,6]). Furthermore, studies such as that of Montecucco [7] solve the heat equation for thermoelectric materials thereby describing its thermal transport behaviour and in turn enabling an analysis of the effectiveness of newly developed materials.

Thermal system management is also necessary to maximize the thermoelectric efficiency of a device since the ability to transfer heat from the heat source to one side of the thermoelectric modules and to transfer heat to the heat sink from the other side of the modules partially dictates the conversion efficiency of the device. Thermal system efficiency studies therefore aim to maximize the thermal dipole across embedded thermoelectric elements by best managing the thermal transfer mechanisms of the available heat source and heat sink. For example, studies such as those of Guo et al. [8] and of Bélanger and Gosselin [9] aim to optimize system thermoelectric power production of a device with embedded commercially available thermoelectric modules by managing the thermal characteristics of flowing fluids. The characteristics of the modules themselves with respect to heat load and electric load are commonly investigated in order to better understand the appropriate working conditions for these thermoelectric converters (e.g., [10,11]). Similarly, Jang et al. [12] describe the optimizing methods for thermoelectric waste-heat recovery of a gaseous flow in which the optimal spacing of the modules over the working surface area is shown to be dependent on the waste gas heat transfer coefficient.

The present work focuses on the thermal management of practical thermoelectric applications. In general, commercially available Bismuth Telluride (Bi_2Te_3) modules are most common in such studies (e.g., [13–15]) since modules containing these alloys have been shown by Karabetoglu et al. [16] and others to have the highest dimensionless Figure-of-Merit values in the temperature range of 273–473 K corresponding well with various low cost heat sources. Such applications include O'Shaughnessy et al.'s [17] thermoelectric biomass cook stove in which the excess heat from a typical wood stove is used to charge an electric battery. In their study, they found that adding ventilation to the cold side of the module enhanced the thermoelectric power offsetting the energy consumption of the ventilation unit. Their study illustrates the importance of managing the entire thermal system of a thermoelectric device.

A growing number of studies focus on the thermal transport mechanisms of flow channels supplying and removing heat from a thermoelectric device (e.g., [18–24]). This is due to the potential to couple a thermoelectric device with large scale industrial liquid-to-liquid heat exchangers which process a non-exploited source of energy. These fluid-to-fluid exchangers expel unwanted heat from the industry environment for operation and safety purposes. Typically, they offer a heat source and heat sink that could supply a thermoelectric device with the necessary thermal dipole if the thermal system were managed such that the power output off-set the pumping penalty. In order to improve the functional efficiency of a thermoelectric liquid-to-liquid generator, Lesage et al. [25] demonstrated that flow impeding channel inserts of specific geometry for a fixed flow rate and varying thermal input conditions can enhance thermopower reaching a 50% net power enhancement when considering the pumping penalty associated with the presence of the obstructing geometries.

The present work builds upon this prospective of enhancing thermal transport in the pipe walls in order to increase power output of a thermoelectric generator. Specifically, a thermoelectric generator is commissioned containing Bi_2Te_3 thermoelectric modules with hot and cold flow channels acting as a heat source and heat sink respectively. The thermal transfer properties associated with geometries made up of alternating flow impeding panels is measured over varying flow rates for fixed thermal input

conditions. The heat transfer enhancement relative to insert geometry and flow rate increases the thermal dipole across the modules thereby increasing thermoelectric power production. Care is taken to measure the adverse pressure drop. Net thermoelectric power output is measured and reported showing a relationship between insert geometry and flow rate for optimal thermoelectric generator operation.

2. Thermoelectric effect

The thermoelectric effect is the onset of charge carrier mobility in an electrical conductor brought upon by an asymmetric thermal field. For descriptive purposes, the thermal field is idealized as a thermal dipole with hot and cold ends. The thermoelectric effect therefore dissipates if the heat conduction through the materials results in a temperature equilibrium at the extremities. Therefore, maintaining the thermal dipole is necessary in any thermoelectric application. Materials are doped to favour either positive or negative charge carriers in order to combine them into thermocouples. A single thermocouple mobilizes charge carriers in the same direction as the flow of heat. Since each pellet leg of the thermocouple is alternately doped, the thermocouple is capable of cycling an electric circuit. Fig. 1 illustrates the thermoelectric phenomenon mobilizing charge carriers in a thermocouple. It is important to note that the management of the heat transfer abilities of the heat source and heat sink is necessary to maintain the thermoelectric phenomenon since heat conduction is also present.

In the present study, the capacity to transfer heat from the heat source and to the heat sink is investigated in a liquid-to-liquid generator with thermoelectric modules.

3. Experimental setup

3.1. Thermoelectric generator

The thermoelectric generator (TEG) of the present study assembled by Thermoelectronics corp. consists of three aluminium plates with embedded aluminium pipes acting as hot and cold water channels. A total of forty commercially available thermoelectric modules (TEMs) TEG2-07025HT-SS are distributed in two layers of twenty and each of the layers is fitted between one hot and one cold surface of the aluminium plates. The TEG's removable inserts with flow impeding panels are illustrated in Fig. 2 along with a general outlook of the generator's assembly.

A total of six pipes with internal diameter of 9.29 mm, for which two channel hot water and four channel cold water as illustrated in Fig. 2. The thermal system is in a hot-cold, counter flow arrangement within the generator which, as detailed [24], provides a more homogeneous $\Delta T = T_H - T_C$ profile the length of the generator. Hot water is divided equally into two sub-flows within the central plate, yielding a symmetrical configuration. The TEMs used measure 40 mm × 40 mm × 4.3 mm each and are composed of alternating p-type and n-type semiconductor pellets of bismuth telluride (Bi_2Ti_3) connected in series and fixed by thin ceramic plates. The TEG measures 472.0 mm × 90.0 mm × 60.0 mm and is covered with machined Styrofoam for thermal insulation.

3.2. Test stand

A test workbench is built in order to measure the influence of different flow turbulence configurations on the output thermoelectric power of the TEG. It channels hot and cold water into the TEG for fixed thermal input conditions over a range of fluid flow rates and for varying flow impeding inserts, creating a thermal dipole with different characteristics over the layers of thermoelectric modules (TEMs). The test stand consists of a thermoelectric generator, a cold water circuit, a hot water circuit and an electrical circuit as shown schematically in Fig. 3.

The hot water circuit is managed by a MicroTherm CMX Series Temperature Control System which combines a pumping and heating system for a controlled heat source flow rate and temperature. For user safety from hot water hazards during TEG operation, a Plexiglas box covers the major connections of the assembly.

Type T thermocouples are used as temperature sensors and are relayed to an Omega RDXL4SD 4-Channel Data logger Thermometer to measure hot and cold inlet and outlet temperatures with an accuracy of ± (0.4% + 0.5 °C). For measuring the fluid flow rate on both the hot and cold circuits, two OMEGA – MR Flow Transmitters are used as sensors connected to the interface ScienceWorkshop 750 and logged using DataStudio software. This data acquisition package is also used to measure the voltage, current and consequently output power dissipated in the external electrical load resistance which is measured to have an impedance of 20.0 ± 0.5% Ω using a Metex M-3800 Digital Multimeter.

The objective of this study is to measure the thermoelectric power gain due to the heat transfer enhancement relative to the associated increase in pressure drop for varying flow rates and varying flow impeding geometries. Ultimately, an optimal insert geometry with respect to flow rate for maximum net power output is investigated. To this end, the pressure is measured for each

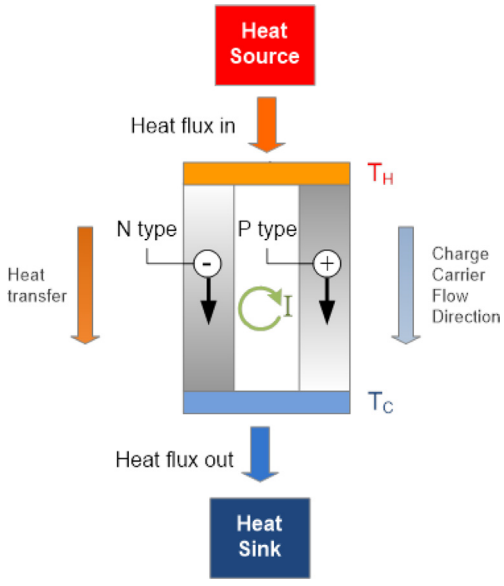

Fig. 1. Thermoelectric effect generating an electric current from a heat source and a heat sink.

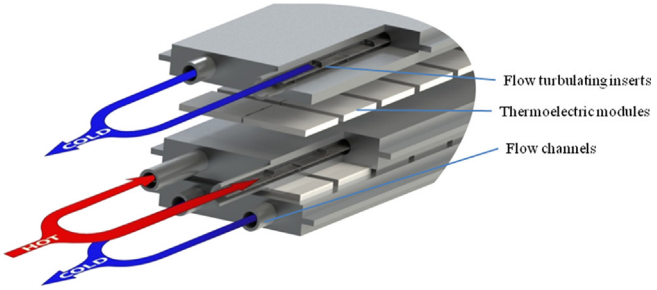

Fig. 2. Generator assembly showing embedded thermoelectric modules and a hot-cold contour flow water circuit.

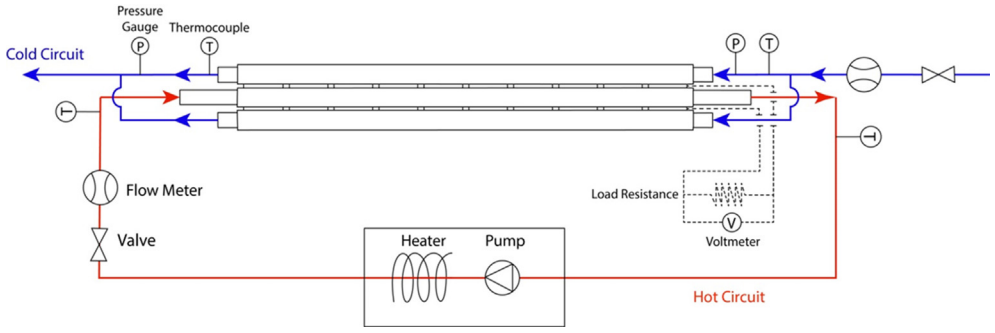

Fig. 3. Schematic representation of the test stand's water and electrical circuit schematic representation.

combination of flow and impeding geometry at the opposing ends of a single channel within the generator. The power gain relative to a reference configuration is calculated taking into account the added power necessary to counter the increased pressure drop. Pressure values are measured using an Omega DPG1001B-100G High-Accuracy Digital Pressure Gauge with a resolution of 0.1 psi and an accuracy of ±0.10%.

3.3. Electrical load resistance

The electric circuit's load resistance is set to approximately 20 Ω since it was shown in Lesage and Pagé-Potvin [24] that for the present generator, an optimal electrical load maximizing power output is within the range of 15.8 Ohms ± 15% which is near electrical impedance matching. This was shown to be true for a wide range of thermal input parameters including a variation in temperature and in flow rates. It was also shown in their study that the descent from peak power for electrical loads greater than optimal is more gradual than that for electrical loads less than optimal. This implies that an error in setting an electrical load inferior to optimal is more costly than an error in setting the electrical load greater than optimal. For this reason a slightly greater than optimal electrical load is imposed on the present work's circuit, as illustrated in Fig. 4.

3.4. Turbulating geometries

In order to create an increasing range of different turbulence conditions, the geometries manufactured from galvanized steel strips with a cross section of 0.50 mm × 8.66 mm are defined by the density of their flow impeding alternating panels. Each steel strip is indexed with reference to the number of panels per metre which are spaced an equidistance from each other. A total of six geometries varying from zero to 125 [panels/m] are commissioned. To certify that all panels have the same shape, a purpose built steel punch and die is used to create each panel of each flow impeding insert. Fig. 5 presents the punch and die tool used to manufacture

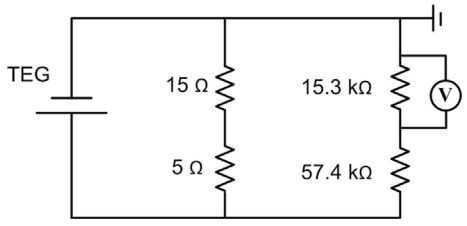

Fig. 4. Electrical circuit of the thermoelectric generator (TEG).

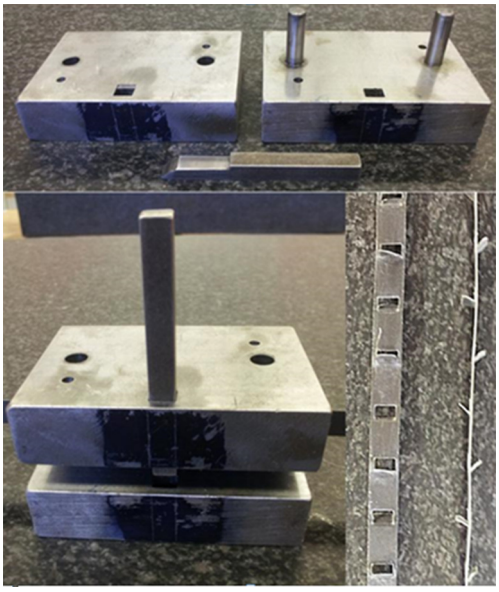

Fig. 5. (Top) Dismantled punch and die tool used to punch equivalent panels in galvanized steel strips; (Bottom left) Assembled punch and die tool; (Bottom right) Flow impeding insert with a panel density of 62.5 panels/m.

the panels and shows a resultant flow impeding galvanized steel insert with 62.5 panels per metre.

In this way, each test case is conducted with respect to two variables: flow ($\dot{V}$ [l/min/channel]) and linear density of panels (D_p [panels/m]). The resulting flow impeding inserts are identified relative to the linear density of panels (D_P) as described in Table 1.

3.5. Measurements

The present work considers the temperature difference between inlet hot water and inlet cold water (ΔT_{in}) as a constant parameter, in order to evaluate the influences of flow rate variations and of flow impeding panel density variations. However, it is not possible

Table 1
List of inserts by panel density.

Flow impeding insert	D_p [Panels/m]
Insert 1	0
Insert 2	7.8
Insert 3	15.6
Insert 4	31.2
Insert 5	62.5
Insert 6	125

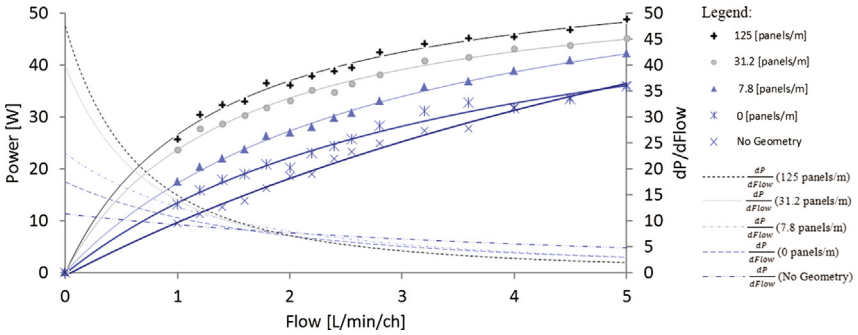

Fig. 6. Thermoelectric power output and its rate of change for varying flow rates and flow impeding inserts.

for the thermal control system to maintain the water temperature in a perfectly static thermal state. For this reason it is necessary to establish a zone of tolerance with respect to the input temperature difference and the aforementioned measuring instrument's uncertainty. The thermal input conditions for all of the test cases presented in this study are maintained within $\overline{\Delta T_{in}} = 70.6 \pm 1.0\ ^{\circ}C$.

4. Results and discussion

4.1. Flow and insert performance comparison

The TEG is first tested over a range of fifteen flow rates in absence of any flow impeding inserts while maintaining the parameter inlet temperature difference between hot and cold flow at 70.6 ± 1.0 °C. The experiment is repeated using all six flow impeding inserts detailed in Table 1. Care is taken to ensure that for each test case, each of the generator's channels is fitted with equivalent insert geometry.

Fig. 6 shows the thermoelectric power output readings with respect to flow rate for TEG operation with varying insert panel density and without flow impeding inserts. Each continuous line represents a fitted curve for constant values of the panel density variable (D_p) with a minimum reliability of 95.5%. It is observed that output power increases with increasing volumetric flow rate per channel and with an increase in panel density. Pertaining to the results illustrated in the following Figs. 6 and 7, the measuring instruments used in this study detailed in Section 2 yield a power output reading with a maximum error of 0.45%.

Although an adverse increase in pressure drop is a result of the presence of the flow impeding inserts and is considered in the following sections, the results of Fig. 6 support the notion that the panels aide in conducting thermal energy through the pipe walls towards (relative to the hot flow channel) or away from (relative to the cold flow channel) the adjacent thermoelectric modules resulting in an increase in power output.

An interesting feature of Fig. 6 is that the rate of increase in power relative to flow rate decreases with increasing flow rates. This is shown by evaluating the power rate of change with respect to flow rate of the best fit curves illustrated in Fig. 6. This is significant since it suggests that the gain in power at higher flow rates may not offset the energy cost of the pumping effort.

Similarly, Fig. 7 shows the same results but from the perspective of thermoelectric power output relative to insert panel density in which each line represents a fitted contour line for constant flow rates. The results reinforce the notion that power output increases for increasing linear panel density (D_P). An important feature of the contours represented in Fig. 7 is that the rate of change of the power output (here represented as dashed lines) decreases for increasing values of the abscissa values. In fact, the thermoelectric power rate of change relative to panel density is shown to converge to zero for all test cases. This implies that for the same input flow rate, beyond a certain panel density D_p there is no further gain in output power.

The power increase discussed is attributed to two principal factors. The first is the increase in flow that maintains a more homogenous thermal field across the thermoelectric modules relative to lower flow rates. This implies that the average temperature difference the length of the TEG is closer to the input temperature difference for higher flow rates. The second contributing factor to thermoelectric power increase is a disturbance in the velocity field brought upon by the flow impeding inserts. This disturbance generates flow patterns in which the axial mean velocity near the channel inner walls increase thereby reducing the thermal boundary layer and improving thermal transport to the adjacent modules. Lesage et al. [25] showed for a fixed flow rate with varying thermal input conditions that the panel's geometry created secondary flows in directions non parallel to the major axial flow thereby preventing the formation of a fully developed inner pipe flow and increasing the radial temperature gradient. This phenomenon is known as the field synergy principal in which thermal enhancement is attributed to a local alignment of the temperature and velocity fields (e.g., [26–29]). It consequently increases the heat flux at the periphery of the flow channel providing an improved heat source on the hot side of the embedded modules and an improved heat sink on their cold side.

4.2. Work due to pressure drop

Although the increasing flow rate and increasing flow impeding panel density raise the thermoelectric power output, they are also responsible for a raise in pressure drop from inlet to outlet of the channel due to increase in friction. This adverse effect adding work to the fluid pump is measured in order to evaluate the net thermoelectric power output. The work due to pressure drop is defined as,

$$\dot{W} = n\Delta p\dot{V} \tag{2}$$

in which n is the number of channels, Δp is the measured pressure drop, and $\dot{V}$ is the fluid flow rate. The results illustrated in Fig. 8 show that the pressure drop increases linearly for increasing flow impeding panel density and that it increases exponentially for increasing fluid flow rate flow rate. This implies that there is a pumping penalty to increasing TEG power by way of an increase in flow rate and an increase in insert panel density.

In considering the 0.1% uncertainty in the pressure gauges at the inlet and the outlet and considering an error due to a unit

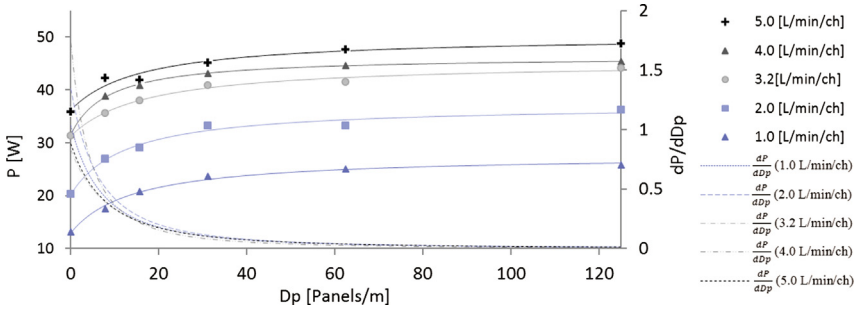

Fig. 7. Thermoelectric power output relative to flow impeding panel density.

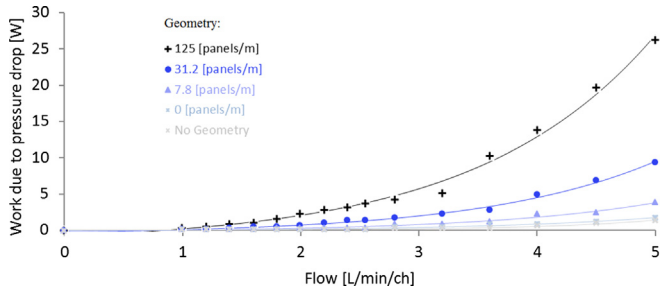

Fig. 8. Work due to pressure drop during TEG operation.

conversion, a resulting maximum error of 6.33% is present in the following pumping penalty results.

It is important to note that in Fig. 8, the work due to the presence of the flow impeding inserts increases exponentially with respect to flow. This and the fact that Fig. 6 shows a power root function behaviour with respect to flow rate suggest that the thermoelectric power enhancement brought upon by the presence of the flow impeding inserts observed will offset the work due to the pressure drop up until an upper flow rate threshold. This threshold is investigated in the following section by analyzing the net thermoelectric power output with respect to flow rate for varying panel densities.

4.3. Net thermoelectric power

The net thermoelectric power is simply the measured TEG power output minus the work due to inner pipe flow. The net thermoelectric power P^{-} is defined as,

$$P^{-} = P - n\Delta p\dot{V} \tag{3}$$

in which P is the total thermoelectric power produced by the generator and the term $n\Delta p\dot{V}$ is the work due to pipe flow. The best fit curves representing the net power generated for varying flow impeding panel densities with respect to flow rate are presented in Fig. 9. The results exhibit local maximums for net thermoelectric power associating an optimal panel density of the geometric form to a flow rate. It is important to note that beyond a threshold flow rate of 5 L/min/ch, the maximum net thermoelectric power output is obtained without any flow impeding inserts. Prior to this threshold flow rate, net power output is greater when TEG operation includes flow impeding inserts. An error analysis resulting from the instruments' measuring tolerance (detailed in Section 2) yields a maximum error of 4.52% for the following net thermoelectric power output results.

By analyzing the net thermoelectric power output relative to panel density for each of the tested flow rates, the peak power of each of the best fit curves associate the optimal panel density to a flow rate. The results of this analysis are illustrated in Fig. 10 which present the optimal panel densities and their associated maximum net thermoelectric power output with respect to flow rate. Evaluating the uncertainty due to the instruments' measuring tolerance reveals a maximum error of 5% for the following optimal panel density results.

The results illustrated in Fig. 10 show that at low flow rates below 3.2 [L/min/ch] the optimal panel density has an approximately constant value of 90 Panels/m as the maximum net thermoelectric power increases in an inverted parabolic manner. Conversely, beyond the flow rate of 3.2 [L/min/ch] the maximum net power remains between 35 and 40 Watts whilst the optimal panel density decreases at a near linear rate with a slope of approximately −50. The decrease in optimal panel density is attributed to the adverse pressure drop brought upon by the panel's flow impedance. Therefore, at higher flow rates, fewer panels produce greater net thermoelectric power. Beyond 5 [L/min/ch], it is shown that the thermal enhancement and power enhancement of the panel inserts does not offset the pumping penalty associated with the presence of the flow impeding inserts and that maximum net thermoelectric power is attained with channel flow free of flow impeding inserts.

4.4. Conversion efficiency

The thermoelectric generator's thermal energy to electrical energy conversion efficiency is calculated by defining the ratio of

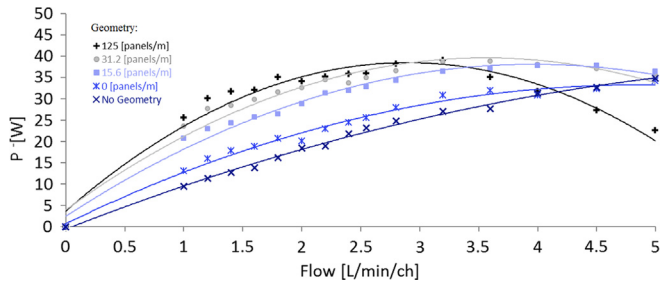

Fig. 9. Net thermoelectric power output accounting for work due to flow impedance.

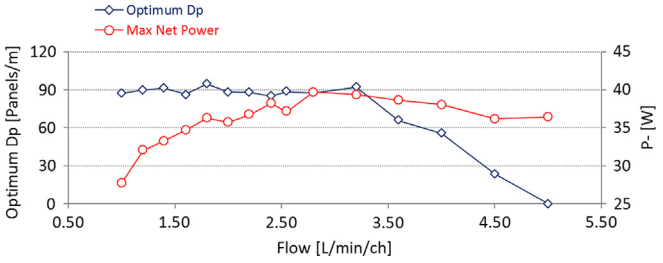

Fig. 10. Optimum panel density D_p for maximum net thermoelectric power P^{-}.

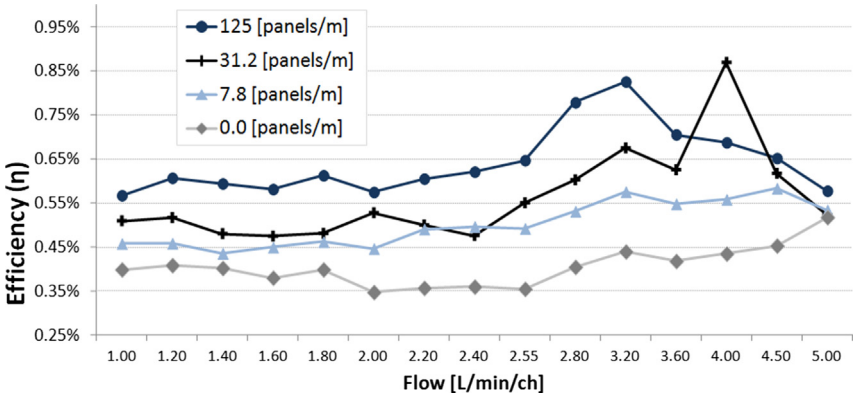

Fig. 11. Thermal energy to electrical energy conversion efficiency over a range of flow rates and using different flow impeding geometries.

the net thermoelectric power output to the thermal energy input as the efficiency parameter. This term is defined in Niu et al. [30] as,

$$\eta = \frac{P^{-}}{\dot{V}\rho_{H}c_{p,H}\Delta T_{H}} \tag{4}$$

in which ρ_H and $c_{p,H}$ are the hot water density and specific heat respectively and ΔT_H is the temperature difference at the inlet and outlet of the hot flow channel. The numerator of Eq. (4) represents the useful electric power produced by the thermoelectric generator and its denominator effectively represents the total thermal energy injected into the generator.

The results of this efficiency calculation for the present generator over varying flow rates and using different flow impeding geometries are illustrated in Fig. 11.

The results illustrated in Fig. 11 show a tendency to a greater conversion efficiency relative to an increase in insert panel density.

5. Conclusion

A thermoelectric liquid-to-liquid generator with forty thermoelectric modules is tested over a variety of flow rates and under different turbulent flow conditions defined by the panel density of flow impeding geometric inserts. For all test cases of the present study, the temperature and pressure in the fluid is recorded at the inlet and outlet of two fluid channels maintained at an input temperature difference of 70.6 °Cs. The thermoelectric power generated due to the resultant asymmetric thermal field is measured for all test operating conditions.

The results show that the measured power output increases for increasing flow rates and for increasing panel density. It is shown that for a fixed flow rate, thermoelectric power output tends to an upper limit for increasing panel density by showing that the rate of change of the best fit curves to the measured power output data with respect to panel density converge to zero.

Furthermore, the adverse work due to flow resistance is measured to increase for increasing insert panel density and that for each insert this work increases exponentially with respect to increasing flow rates. This observation along with the measured root function power output curve relative to flow rate suggest that an upper flow rate threshold exists beyond which the thermoelectric power enhancement brought upon by the flow impeding inserts no longer offsets the work due to the pressure drop. This is confirmed by way of an evaluation of the net thermoelectric power output which is simply the power output minus the work due to the pressure drop. It is shown that the net thermoelectric power output behaves in an inverted parabolic manner with respect to flow rate and that flow impeding panel inserts yield a greater net thermoelectric power than an absence of inserts up to a threshold flow rate. Also, optimal insert panel density values maximizing the net thermoelectric power output are identified with respect to flow rate.

In conclusion, it is shown that channel inserts with alternating flow impeding panels enhance thermoelectric power production offsetting any pumping penalty due to their presence up to a threshold flow rate for given working conditions.

Acknowledgements

The authors gratefully thank the Fondation du Cégep de l'Outaouais, the Brazilian Conselho Nacional de Desenvolvimento Científico e Tecnológico (CPNq), and the Canadian Bureau for International Education (CBIE) for their generous support throughout this project. The authors also thank Rémi Pelletier for his exceptional technical expertise.

References

[1] C. Wu, Analysis of waste-heat thermoelectric power generators, Appl. Therm. Eng. 16 (1996) 63–69.
[2] D.M. Rowe, Thermoelectrics Handbook Macro to Nano, Taylor & Francis, London, 2006.
[3] C. André, D. Vasilevskiy, S. Turenne, R.A. Masut, Extruded bismuth-telluride-based n-type alloys for waste heat thermoelectric recovery applications, J. Electron Mater. 38 (2009) 1061–1067.
[4] P.F.P. Poudeu, A. Guéguen, C.-I. Wu, T. Hogan, M.G. Kanatzidis, High Figure of Merit in Nanostructured n-type HPb_mSbTe_{m+2} thermoelectric materials, Chem. Mater. 22 (2010) 1046–1053.
[5] D. Ebling, K. Bartholomé, M. Bartel, M. Jägle, Module geometry and contact resistance of thermoelectric generators analyzed by multiphysics simulation, J. Electron Mater. 39 (2010) 1376–1380.
[6] C. Hadjistassou, E. Kyriakides, J. Georgiou, Designing high efficiency segmented thermoelectric generators, Energy Convers. Manage. 66 (2013) 165–172.
[7] A. Montecucco, J.R. Buckle, A.R. Knox, Solution to the 1-D unsteady heat conduction equation with internal Joule heat generation for thermoelectric devices, Appl. Therm. Eng. 35 (2012) 177–184.
[8] X. Gou, H. Xiao, S. Yang, Modeling, experimental study and optimization on low temperature waste heat thermoelectric generator system, Appl. Energy 87 (2010) 3131–3136.
[9] S. Bélanger, L. Gosselin, Thermoelectric generator sandwiched in a crossflow heat exchanger with optimal connectivity between modules, Energy Convers. Manage. 52 (2012) 2911–2918.
[10] R. Palacios, A. Arenas, R.R. Pecharromán, F.L. Pagola, Analytical procedure to obtain internal parameters from performance curves of commercial thermoelectric modules, Appl. Therm. Eng. 29 (2009) 3501–3505.
[11] F.J. Lesage, R. Pelletier, L. Fournier, E. Sempels, Optimal electrical load for peak power of a thermoelectric module with a solar electric application, Energy Convers. Manage. 74 (2013) 51–59.
[12] J.Y. Jang, Y.C. Tsai, Optimization of thermoelectric generator module spacing and spreader thickness used in a waste heat recovery system, Appl. Therm. Eng. 51 (2013) 677–689.

[13] D.T. Crane, G.S. Jackson, Optimization of cross flow heat exchangers for thermoelectric waste heat recovery, Energy Convers. Manage. 45 (2004) 1565–1582.
[14] A. Rodriguez, J.G. Vian, D. Astrain, A. Martinez, Study of thermoelectric systems applied to electric power generation, Energy Convers. Manage. 50 (2009) 1236–1243.
[15] S.A. Whalena, R.C. Dykhuizenb, Thermoelectric energy harvesting from diurnal heat flow in the upper soil layer, Energy Convers. Manage. 64 (2012) 397–402.
[16] S. Karabetoglu, A. Sisman, Z. Faith Ozturk, T. Sahin, Characterization of a thermoelectric generator at low temperatures, Energy Convers. Manage. 62 (2012) 47–50.
[17] S.M.O. 'Shaughnessy, M.J. Deasy, C.E. Kinsella, J.V. Doyle, A.J. Robinson, Small scale electricity generation from a portable biomass cookstove: prototype design and preliminary results, Appl. Energy 102 (2013) 374–385.
[18] J.W. Stevens, Optimal design of small ΔT thermoelectric generation systems, Energy Convers. Manage. 42 (2001) 709–720.
[19] C. Yu, K.T. Chau, Thermoelectric automotive waste heat energy recovery using maximum power point tracking, Energy Convers. Manage. 50 (2009) 1506–1512.
[20] E.W. Miller, T.J. Hendricks, R.B. Peterson, Modeling energy recovery using thermoelectric conversion integrated with an organic rankine bottoming cycle, J. Electron Mater. 38 (2009) 1206–1213.
[21] D. Dai, Y. Zhou, J. Liu, Liquid metal based thermoelectric generation system for waste heat recovery, Renew. Energy 36 (2011) 3530–3536.
[22] N.R. Kristiansen, G.J. Snyder, H.K. Nielsen, L. Rosendahl, Waste heat recovery from a marine waste incinerator using a thermoelectric generator, J. Electron Mater. 41 (2012) 1024–1029.
[23] T.J. Hendricks, N.K. Karri, T.P. Hogan, C.J. Cauchy, New perspectives in thermoelectric energy recovery system design optimization, J. Electron Mater. (2013) 1–12.
[24] F.J. Lesage, N. Pagé-Potvin, Experimental analysis of peak power output of a thermoelectric liquid-to-liquid generator under an increasing electrical load resistance, Energy Convers. Manage. 66 (2013) 98–105.
[25] F.J. Lesage, E.V. Sempels, N. Lalande-Bertrand, A study on heat transfer enhancement using flow channel inserts for thermoelectric power generation, Energy Convers. Manage. 75 (2013) 532–541.
[26] J.M. Wu, W.Q. Tao, Investigation on laminar convection heat transfer in fin-and-tube heat exchanger in aligned arrangement with longitudinal vortex generator from the viewpoint of field synergy principle, Appl. Therm. Eng. 27 (2007) 2609–2617.
[27] Y.P. Cheng, T.S. Lee, H.T. Low, Numerical simulation of conjugate heat transfer in electronic cooling and analysis based on field synergy principle, Appl. Therm. Eng. 28 (2008) 1826–1833.
[28] J. Li, H. Peng, X. Ling, Numerical study and experimental verification of transverse direction type serrated fins and field synergy principle analysis, Appl. Therm. Eng. 54 (2013) 328–335.
[29] Y. Li, J. Wu, L. Zhang, L. Kou, Comparison of fluid flow and heat transfer behavior in outer and inner half coil jackets and field synergy analysis, Appl. Therm. Eng. 31 (2011) 3078–3083.
[30] X. Niu, J. Yu, S. Wang, Experimental study on low-temperature waste heat thermoelectric generator, J. Power Sources 188 (2009) 621–626.